Journal for
ImmunoTherapy of Cancer

Development and validation of the immune signature to predict distant metastasis in patients with nasopharyngeal carcinoma

Sai-Lan Liu,[1,2] Li-Juan Bian,[3] Ze-Xian Liu,[1] Qiu-Yan Chen,[1,2] Xue-Song Sun,[1,2] Rui Sun,[1,2] Dong-Hua Luo,[1,2] Xiao-Yun Li,[1,2] Bei-Bei Xiao,[1,2] Jin-Jie Yan,[1,2] Zi-Jian Lu,[1,2] Shu-Mei Yan,[1,4] Li Yuan,[1,2] Lin-Quan Tang,[1,2] Jian-Ming Li,[3] Hai-Qiang Mai [ID] [1,2]

ABSTRACT

Background The tumor immune microenvironment has clinicopathological significance in predicting prognosis and therapeutic efficacy. We aimed to develop an immune signature to predict distant metastasis in patients with nasopharyngeal carcinoma (NPC).

Methods Using multiplexed quantitative fluorescence, we detected 17 immune biomarkers in a primary screening cohort of 54 NPC tissues presenting with/without distant metastasis following radical therapy. The LASSO (least absolute shrinkage and selection operator) logistic regression model used statistically significant survival markers in the training cohort (n=194) to build an immune signature. The prognostic and predictive accuracy of it was validated in an external independent group of 304 patients.

Results Eight statistically significant markers were identified in the screening cohort. The immune signature consisting of four immune markers (PD-L1+ CD163+, CXCR5, CD117) in intratumor was adopted to classify patients into high and low risk in the training cohort and it showed a high level of reproducibility between different batches of samples (r=0.988 for intratumor; p<0.0001). High-risk patients had shorter distant metastasis-free survival (HR 5.608, 95% CI 2.619 to 12.006; p<0.0001) and progression-free survival (HR 2.798, 95% CI 1.498 to 5.266; p=0·001). The C-indexes which reflected the predictive capacity in training and validation cohort were 0.703 and 0.636, respectively. Low-risk patients benefited from induction chemotherapy plus concurrent chemoradiotherapy (IC+CCRT) (HR 0.355, 95% CI 0.147 to 0.857; p=0·021), while high-risk patients did not (HR 1.329, 95% CI 0.543 to 3.253; p=0·533). To predict the individual risk of distant metastasis, nomograms with the integration of both immune signature and clinicopathological risk factors were developed.

Conclusions The immune signature provided a reliable estimate of distant metastasis risk in patients with NPC and might be applied to identify the cohort which benefit from IC+CCRT.

INTRODUCTION

In South China, nasopharyngeal carcinoma (NPC) is one of the most prevalent cancers.[1 2]

Of the 87 000 newly diagnosed cases of NPC each year, more than 70% are locoregionally advanced disease.[3] The prevention of distant metastasis, which is the main reason for treatment failure in advanced NPC remains unsatisfactory.[4] The currently applied method for guiding treatment and predicting prognosis is mainly based on the tumor–node–metastases (TNM) staging system, which only take anatomical data into consideration and is insufficient to predict distant metastasis. Therefore, more precise diagnostic measures and effective treatments are required to guide individual treatment for patients with NPC.

Emerging evidence demonstrates that the specific tumor microenvironment could promote tumor progression and the diversity of its characteristics could be used for molecular classification, prediction of treatment responses and prognosis in a variety of cancers.[5–7] NPC is characterized by abundant immunocell infiltration in the primary tumor, including T cells, B cells, mast cells (MCs), macrophages, and neutrophils.[8] Previous studies suggested the adverse effects of the increase in macrophage, MCs, and neutrophils infiltration, which could play important roles in tumor support.[9–11] In the meantime, many studies have reported that non-malignant lymphocytes infiltrating into the tumor and stroma was associated with favorable prognostic effects.[12 13] However, the antitumor response of these lymphocytes was often suppressed by immune checkpoints. Among them, programmed cell death-1 (PD-1) and T-cell immunoglobulin and mucin domain-containing protein 3 (TIM-3) were well-known immune checkpoints that hindered the function of activated T cells by mainly connecting programmed death-ligand

1 (PD-L1) and galectin-9, respectively.[14 15] In addition, lymphocyte-activation gene 3 (LAG-3) and galectin-1 were novel tumor immunotherapeutic targets, which recently attracted enormous attention.[16 17] These immune cells and immune checkpoints might serve as important identifiers permitting early diagnosis and subgroup classification.[18 19] The previous studies on immune microenvironment of NPC were mostly presented with small sample size and an absence of independent validation, and mainly focused on limited number of markers. Besides, the coexpression of markers and the characteristics of non-malignant cells were often neglected. Since both malignant cells and stromal cells orchestrate in tumor-associated inflammation, tumor progression, and metastasis,[20] it is of great necessity to picture the whole landscape of tumor immune microenvironment and pay attention to their relative locations. Furthermore, the difference in immune patterns among patients with various clinical outcomes, particularly distant metastasis should also be concerned and emphasized.

Cell-specific and topological analysis of immune checkpoint expression and immune cells in patients has become feasible with the development of fluorescent multiplex immunohistochemistry (IHC) and automated quantitation technology, which offers more objective perspectives and provides better prognostic information compared with conventional IHC-based pathological estimation.[21 22] In the present study, a MultiOmyx platform was used to perform coexpression analysis and phenotype identification by integrating results from individual markers. In that case, we could simultaneously quantify the expression of 17 immune markers in intratumor and stromal tissues, including 6 important immune checkpoint molecules (PD-1, PD-L1, TIM-3, galectin-9, LAG-3, and galectin-1), and 11 relevant prognostic leukocyte markers: mature T lymphocytes (CD3), helper T cells (CD4), cytotoxic T cells (CD8), neutrophils (CD66b), T-cell follicular helper cells (CXCR5), regulatory T cells (Tregs) Foxp3+, monocytes (CD68), M2 macrophages (CD163), type 1 helper T cells (T-bet), and MCs (CD117), in a large cohort of NPC cases. The prediction of distant metastasis in patients with NPC can be further achieved by identifying and validating the immune signature. Moreover, we produced more accurate nomogram models for distant metastasis by integrating the immune signature with other clinical risk factors.

PATIENTS AND METHODS
Study population
The study workflow is shown in figure 1. The present study used the following eligibility criteria[1]: newly diagnosed stage II–IVa NPC[2]; did not receive any antitumor therapy before biopsy sampling[3]; received radical intensity modulated radiotherapy (IMRT) with or without chemotherapy[4]; age ≥18 years; Eastern Cooperative
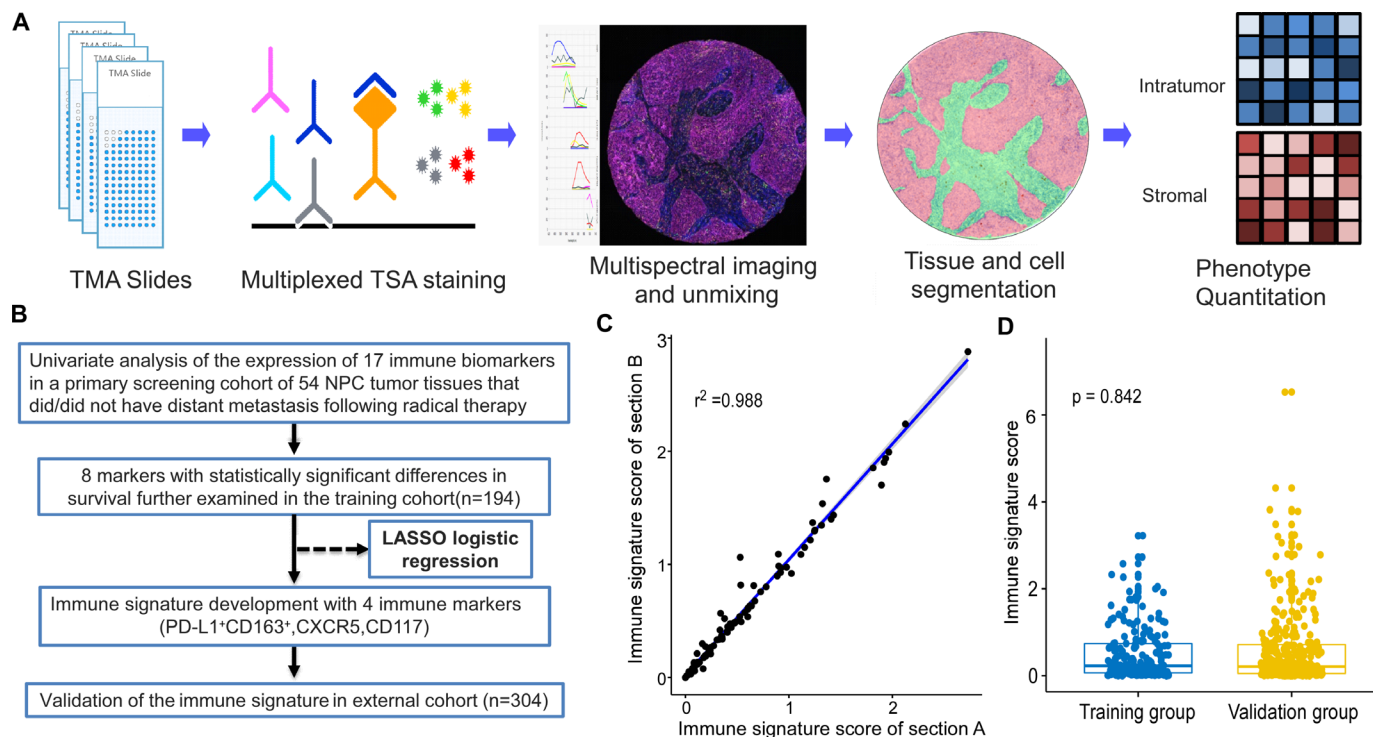
Figure 1 Workflow of the present study. (A) Process of multiplexed immunofluorescence staining and image analysis. (B) Study flow. (C) Example of a 2×2 correlation of the immune signature in the intratumor between two continuous sections of TMAs (r=0.988). (D) Scatter diagram illustrating the immune signature A of the training and validation cohorts. Statistical comparison was performed by first testing normality using the Kolmogorov-Smirnov test, and then the Mann-Whitney non-parametric test was used to compare the two groups. LASSO, least absolute shrinkage and selection operator; NPC, nasopharyngeal carcinoma; TMA, tissue microarray; TSA, tyramide signal amplification.

Oncology Group (ECOG) score between 0 and 2[5]; adequate hematological, renal, and hepatic functions; and[6] no concomitant pregnancy, lactation, and other malignant disease. Between October 20, 2010 and March 16, 2016, 194 samples were obtained from patients treated at the Sun Yat-sen University Cancer Center (Guangzhou, China). As the external validation cohort, 304 samples were obtained from the Sun Yat-sen Memorial Hospital (Guangzhou, China) between December 12, 2011 and September 1, 2015. The eighth edition of the American Joint Committee on Cancer Staging Manual was used to restage all the patients. Theonline supplementary file 6(p1) showed detailed information concerning the radiotherapy dose and chemotherapy regimens. The plasma Epstein–Barr virus (EBV) DNA concentrations of patients were measured by quantitative PCR as described in the online supplementary file 6 (p 1, 2).

Multiplexed immunofluorescence staining

One 1.0 mm tissue core from intratumor area was used to construct the tissue microarrays (TMAs), and another selected tissue core was available to locate stromal regions if possible in training cohort and one 1.0 mm tissue core from intratumor area was used to construct the TMAs in validation cohort. All tissue cores were reassessed by two pathologists (L-JB and S-MY), and tissue cores containing more than 70% tumor cells or stromal cells were included for further analysis, so the total area of intratumor and stromal tissue analyzed in each case was more than $0.55\,mm^2$. All immunofluorescence staining was carried out on 4-µm-thick formalin-fixed, paraffin-embedded TMAs. In the present study, we selected 17 prognostic markers mentioned earlier in this article for immunofluorescence staining of NPC tissues according to their involvement in cancer prognosis.[9 13 23–30] The biomarkers' names, antibody dilutions, and antibody clones are presented in online supplementary table 1. online supplementary file 6 (p 2,3) detailed the method about validation and standardization of antibodies. PANO 7-plex IHC kit, cat 0004100100 (Panovue, Beijing, China) was used according to the manufacturer's protocol. Briefly, TMAs embedded in paraffin were deparaffinized, rehydrated, and subjected to antigen retrieval buffer treatment. Antigen retrieval was performed by microwave treatment in basic (EDTA, pH 9.0) antigen retrieval buffer. To block the endogenous peroxide activity, the sections were incubated in 3% hydrogen peroxide for 10 min at room temperature, followed by washing in 1×Tris-buffered saline–Tween 20. The sections were then incubated with each primary antibody separately for 60 min. After washing, the sections were incubated for 10 min with a rabbit or mouse probe antibody specific for the species of the primary antibody, washed, and then incubated with a rabbit or mouse horseradish peroxidase conjugated secondary antibody for a further 10 min. The sections were then washed and incubated with opal fluorophores (1:100 dilution in tyramide signal amplification reagent from the opal kit). For each additional marker,

the protocol was repeated by treating the slides with an antigen retrieval step, followed by primary antibody staining and the subsequent downstream steps. Finally, all sections were stained using 2-(4-amidinophenyl)-1H-indole-6-carboxamidine (D9542, Sigma-Aldrich) for 3 min. The sections were imaged under a fluorescent microscope fitted with an automated quantitative pathology imaging system called Polaris System (PerkinElmer, Waltham, Massachusetts, USA). Images were unmixed and annotated using inForm image analysis software (V.2.4, PerkinElmer). A combination of the percentage and intensity of positively stained cells was used to score the immune markers to generate a histochemistry (H)-score.[31] online supplementary file 6 (p 3–5) detailed the process of identification of intratumor and stromal tissue and the multispectral imaging and scoring standard for the immune markers.

Statistical analysis

The H-score or percentage of immune cells obtained from all available cores in the intratumor and stromal tissues of each case were used. We first compared 54 patients with patients with NPC at the Sun Yat-sen University Cancer Center with metastasis (n=25) or without metastasis (n=29) after radical therapy as the original training group. This group was well balanced in terms of T stage, gender, age, N stage, and treatment method, which eliminated the effect of these factors on metastasis (online supplementary table 2). Univariate analyses using Cox proportional hazards regression modeling was then used to test the significance of different immune markers in this original training group. The p-value for significant markers (<0.05) remained for further validation within the training group.

To construct a prediction model in the training group, we used a penalized logistic model to select markers. The coefficients weighted by the penalized logistic model were used to construct the prediction model using the R package glmnet in the training cohort (online supplementary file 6 (p 5)). In the training cohort, the X-tile software (V.3.6.1; Yale University, New Haven, Connecticut, USA), which can automatically select the optimum data threshold according to the highest χ^2 value (minimum p value) defined by Kaplan-Meier survival analysis and logrank test[32] was used to identify the optimal cut-off value.

Distant metastasis-free survival (DMFS) was the primary endpoint, defined as the interval between the first day of diagnosis to the advent of first distant metastasis event. Progression-free survival (PFS) was the secondary endpoint, defined as the interval between the first date of diagnosis and disease progression or death from any cause. The Kaplan-Meier method was used to analyze survival, and the log-rank test was used to compare the differences between groups. We calculated the HRs using univariate Cox regression analysis. As a predictor of benefit gained from induction chemotherapy plus concurrent chemoradiotherapy (IC+CCRT), the immune

signature was analyzed in the combined training and external cohorts.

Multivariate Cox regression analysis with backward selection was performed to test the independent significance of different variables. To remove non-significant variables from the analysis, the threshold p value was set at 0.1 (p>0.1), and the final Cox model retained marginally significant variables (005<p<0.1). The following covariates were involved in the model, including the immune signature (high risk vs low risk), gender (male vs female), age (≥45 years vs <45 years), T stage (T3–4 vs T1–2), N stage (N2–3 vs N0–1), ECOG (0 vs 1 vs 2), serum lactate dehydrogenase (≥245 vs <245 U/L), C reactive protein (≥3.0 vs <3.0 mg/L), hemoglobin (HGB;<130 vs ≥130 g/L) and body mass index (≥23 vs <23 kg/m²). For the multivariable Cox regression model, the coefficients were used to construct nomograms. The calibration curves were made by plotting the observed rates against the predicted probabilities of nomogram. A bootstrapping method with 1000 resamples was used to calculate the concordance index (C-index). To evaluate the prognostic or predictive accuracy of the clinical features and the immune signature-based nomogram, receiver operating characteristic (ROC) analysis was used. The area under the ROC curve was calculated to assess the sensitivity and specificity of the model to predict distant metastasis. All statistical analyses were performed using R (V.3.6.0) and SPSS (V.22.0, IBM). The statistical tests were all two-sided, and statistical significance was indicated by a p-value of less than 0.05.

RESULTS
Patient characteristics
Table 1 summarized the patient characteristics in the training cohort (n=194) and external validation cohort (n=304). The patients had a median age of 46 years (range: 18–78) years. There were 150 (30.1 %) female patients and 348 (69.9%) male patients. Seventy-five (15.1%) patients were diagnosed with stage II disease, 252 (50·6%) with stage III, and 171 (34.3%) with stage IVa. All 498 patients underwent radical IMRT. Additionally, among them, 201 (40.4%) received IC plus CCRT and 187 (37.6%) received CCRT alone. The median follow-up was 62.0 months (IQR 26.1–60.2), and 62 (12.4%) of the 498 patients developed distant metastasis during the follow-up period.

Screening results of the primary training group
Data for 54 intratumor cores and 40 stromal cores containing more than 70% tumor cells or stromal cells from 54 specimens of the primary training cohort were used for further analysis. We used the median H-score or percentage as a cut-off score and found that the expression of LAG-3 and CD117 in the intratumor region were individually associated with DMFS. In addition, the ratio of TIM-3$^+$ CD8$^+$ T cells and PD-L1$^+$CD163$^+$ cells yielded strong negative associations with DMFS and the ratio of

PD-1$^+$ CD8$^+$ T cells and CD39$^+$CD8$^+$cells had no significant correlation with DMFS. As regard to stromal cells, high expression of CXCR5 and Foxp3 were identified with poorer DMFS (online supplementary table 3). The above eight significant immune markers (TIM-3, CD8, PD-L1, CD163, LAG-3, CXCR5, Foxp3, and CD117) were adopted for further verification using the training cohort of 194 patients. The eight selected immune markers showed distinguishable and clear staining as shown in online supplementary figure 1.

Association of the immune signature with prognosis
The least absolute shrinkage and selection operator (LASSO) logistic regression model was used to build prognostic immune signature A, which involved four markers in intratumor (percentage of PD-L1$^+$ CD163$^+$, CXCR5, CD117) identified by the training set (n=194) (online supplementary figure 2). The immune signature of each patient was calculated based on their regression coefficients of the expression levels of these immune markers in the intratumor (online supplementary table 4): Immune signature A= (0.013479×1000×percentage of PD-L1$^+$ CD163 $^+$)+(0.057512×H-score of CXCR5)+(0.011048×H-score of CD117). Immunofluorescence staining was carried out on two continuous sections of TMAs and it showed strong repeatability and reproducibility between different batches (r=0.988 for intratumor; p<0.0001; figure 1C). In the training cohort, the patients were separated into low-risk and high-risk groups using an optimal cut-off value generated by X-tile plots (online supplementary figure 3). The low-risk and high-risk group, respectively, comprised 78.4% (152/194) and 21.6% (42/194) of the patients. The 5-year DMFS was 61.4% (95% CI 45.9% to 76.9%) in the high-risk group and 89.1% (95% CI 82.2% to 96.0%) in the low-risk group (HR 5.608, 95% CI 2.619 to 12.006; p<0.0001; figure 2; online supplementary table 5). Patients in the high-risk group also had shorter PFS values (HR 2.798, 95% CI 1.498 to 5.226; p=0.001; figure 2; online supplementary table 5) compared with that in the low-risk group.

Both malignant cells and stromal cells orchestrated in tumor progression and metastasis. Therefore, we developed immune signature B by taking both intratumor and stromal conditions into consideration and found no statistically significant difference between immune signature B and immune signature A (data not shown). Obtained by biopsy forceps, the NPC tissue was too tiny for every tissue section to contain enough stromal tissue to construct TMA and there were only 65.5% (127/194) of patients with available data for stromal cores in our study, which indicated a limited application value of immune signature B in clinical practice. Given the better accessibility and similar prognostic value of immune signature A, it was selected to predict the prognosis of patients with NPC in validation cohort. A scatter diagram illustrating the immune signature of the training and validation cohorts was shown in figure 1D with no significant difference in immune signature distribution observed between the

Table 1 Clinical characteristics of patients in the training and external validation cohorts

	Training cohort (N=194)			Validation cohort (N=304)		
	Patients (n)	Low-risk	High-risk	Patients (n)	Low-risk	High-risk
Age (years)						
<45	100 (51.5)	74 (74.0)	26 (26.0)	121 (39.8)	93 (76.9)	28 (23.1)
≥45	94 (48.5)	78 (83.0)	16 (17.0)	183 (60.2)	141 (77.0)	42 (23.0)
Sex						
Male	133 (68.6)	102 (76.7)	31 (23.3)	215 (70.7)	163 (75.8)	52 (24.2)
Female	61 (31.4)	50 (82.0)	11 (18.0)	89 (29.3)	71 (79.8)	18 (20.2)
Pathological type						
WHO II	4 (2.1)	3 (75.0)	1 (25.0)	9 (3.0)	8 (88.9)	1 (11.1)
WHO III	190 (97.9)	149 (78.4)	41 (21.6)	295 (97.0)	226 (76.6)	69 (23.4)
T stage*						
T1	9 (4.6)	6 (66.7)	3 (33.3)	28 (9.2)	24 (85.7)	4 (14.3)
T2	34 (17.5)	25 (73.5)	9 (26.5)	111 (36.5)	88 (79.3)	23 (20.7)
T3	109 (56.2)	88 (80.7)	21 (19.3)	98 (32.2)	71 (72.4)	27 (27.6)
T4	42 (21.6)	33 (78.6)	9 (21.4)	67 (22.0)	51 (76.1)	16 (23.9)
N stage*						
N0	9 (4.6)	9 (100.0)	0 (0.0)	27 (8.9)	22 (81.5)	5 (18.5)
N1	81 (41.8)	64 (79.0)	17 (21.0)	108 (35.5)	79 (73.1)	29 (26.9)
N2	75 (38.7)	56 (74.7)	19 (25.3)	130 (42.8)	103 (79.2)	27 (20.8)
N3	29 (14.9)	23 (79.3)	6 (20.7)	39 (12.8)	30 (76.9)	9 (23.1)
TNM stage*						
II	21 (10.8)	15 (71.4)	6 (28.6)	54 (17.8)	43 (79.6)	11 (20.4)
III	106 (54.6)	84 (79.2)	22 (20.8)	146 (48.0)	112 (76.7)	34 (23.3)
IV	67 (34.5)	53 (79.1)	14 (20.9)	104 (34.2)	79 (76.0)	25 (24.0)
EBV DNA (copies/mL)						
≥1500	102 (52.6)	76 (74.5)	26 (25.5)	NA	NA	NA
<1500	92 (47.7)	76 (82.6)	16 (17.4)	NA	NA	NA
ECOG						
0	15 (7.7)	11 (73.3)	4 (26.7)	20 (6.6)	15 (75.0)	5 (25.0)
1	172 (88.7)	136 (79.1)	36 (20.9)	267 (87.8)	205 (76.8)	62 (23.2)
2	7 (3.6)	5 (71.4)	2 (28.6)	17 (5.6)	14 (82.4)	3 (17.6)
LDH concentration (U/L)						
<245	177 (91.2)	139 (78.5)	38 (21.5)	265 (87.2)	209 (78.9)	56 (21.1)
≥245	17 (8.8)	13 (76.5)	4 (23.5)	39 (12.8)	25 (64.1)	14 (35.9)
C reactive protein concentration (mg/L)						
<3.0	131 (67.5)	102 (77.9)	29 (22.1)	190 (62.5)	148 (77.9)	42 (22.1)
≥3.0	63 (32.5)	50 (79.4)	13 (20.6)	114 (37.5)	86 (75.4)	28 (24.6)
Hemoglobin concentration (g/L)						
<130	44 (22.7)	39 (88.6)	5 (11.4)	93 (30.6)	71 (76.3)	22 (23.7)
≥130	150 (77.3)	113 (75.3)	37 (24.7)	211 (69.4)	163 (77.3)	48 (22.7)
Body mass index (kg/m²)						
<23.0	107 (55.2)	83 (77.6)	24 (22.4)	177 (58.2)	139 (78.5)	38 (21.5)
≥23.0	87 (44.8)	69 (79.3)	18 (20.7)	127 (41.8)	95 (74.8)	32 (25.2)
Treatment method						
CCRT	78 (40.2)	63 (80.8)	15 (19.2)	109 (35.9)	83 (76.1)	26 (23.9)
IC+CCRT	89 (45.9)	70 (78.7)	19 (21.3)	112 (36.8)	87 (77.7)	25 (22.3)
RT/IC+RT/CCRT+AC	27 (13.9)	19 (70.4)	8 (29.6)	83 (27.3)	64 (77.1)	19 (22.9)

*According to the eighth edition of UICC/AJCC staging system.
AC, adjuvant chemotherapy; AJCC, American Joint Committee on Cancer; CCRT, concurrent chemoradiotherapy; EBV, Epstein–Barr virus; ECOG, Eastern Cooperative Oncology Group; IC, induction chemotherapy; LDH, serum lactate dehydrogenase; NA, not available; RT, radiotherapy; TNM, tumor–node–metastases; UICC, Union for International Cancer Control.
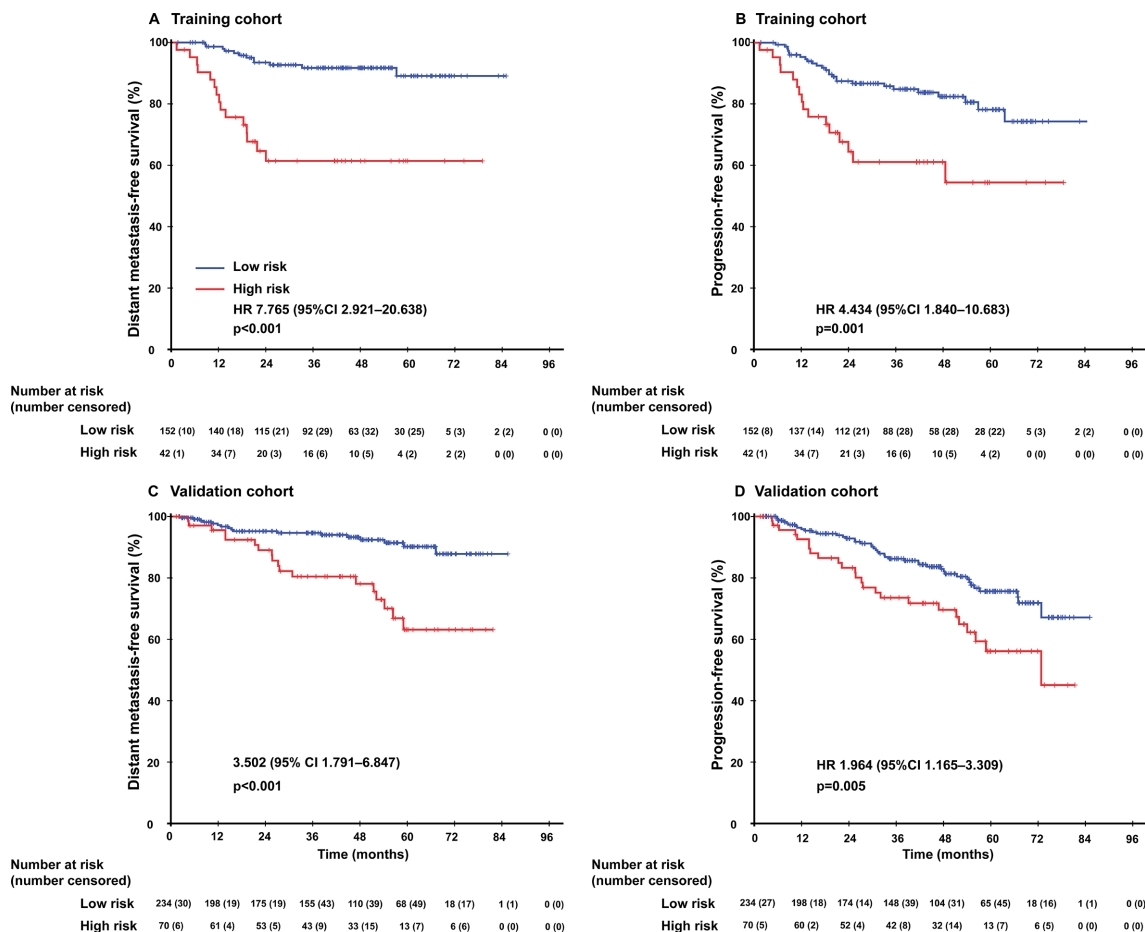
Figure 2 Kaplan-Meier curves for distant metastasis-free survival and progression-free survival between the immune signature-defined high-risk and low-risk groups in the training and validation cohorts.

two groups (p=0.842). In the validation cohort, immune signature A categorized 234 (81.3%) of the 304 patients into low-risk group and 70 patients (18.7%) into high-risk group. Patients in high-risk group demonstrated with far shorter DMFS (HR 3.502, 95% CI 1.791 to 6.847; p<0.0001; figure 2, online supplementary table S5) and PFS (HR 1.964, 95% CI 1.165 to 3.309; p=0.011; figure 2, online supplementary table S5) in contrary to low-risk patients.

Benefit of induction chemotherapy

Among the 498 patients in the combined cohort, 167 (33.5%) received CCRT and 221 (44.8%) received IC+CCRT. For these patients, survival outcomes were comparable between IC+CCRT and CCRT alone groups (figure 3). Then, the immune signature was applied to predict the survival benefit gained from IC. Stratification of immune signature A with Kaplan-Meier survival analysis showed that treatment with IC+CCRT rather than CCRT was associated with improved DMFS (HR 0.355, 95% CI 0.147 to 0.857; p=0.021) and PFS (HR 0.590, 95% CI 0.351 to 0.992; p=0.047) in patients with low immune signature scores rather than those with high immune signature scores (DMFS: HR 1.294, 95% CI 0.553 to 3.029; p=0.552; PFS: HR 1.248, 95% CI 0.590 to 2.639; p=0.563; figure 3).

Online supplementary table S6 in the appendix showed the 5-year DMFS and PFS in each risk group.

Establishment and validation of nomograms with the immune signature

After multivariable adjustment by clinicopathological risk factors, immune signature A remained a strong independent prognostic factor for DMFS in the training cohort (HR 6.295, 95% CI 2.886 to 13.729; p<0.0001; table 2) and in the validation cohort (HR 4.297, 95% CI 2.182 to 8.461; p<0.001; table 2). In addition, N stage (HR 2.522, 95% CI 1.086 to 5.857; p=0.031) and HGB (HR 0.335, 95% CI 0.126 to 0.890; p=0.028) also remained significant for DMFS after adjustment for various cofactors. Among them, immune signature A had the highest C-index (0.703, 95% CI 0.613 to 0.793; C-index 0.636, 95% CI 0.551 to 0.721) both in training and validation cohort (online supplementary table S7). Then, we constructed nomogram A to predict the 5-year DMFS by combining the variables of immune signature A, N stage, and pretreatment HGB levels (figure 4). The calibration plots for the nomogram A were predicted well in the training cohort (C-index 0.791, 95% CI 0.720 to 0.862) and the validation cohort (C-index 0.729, 95% CI 0.630 to 0.828; figure 4).
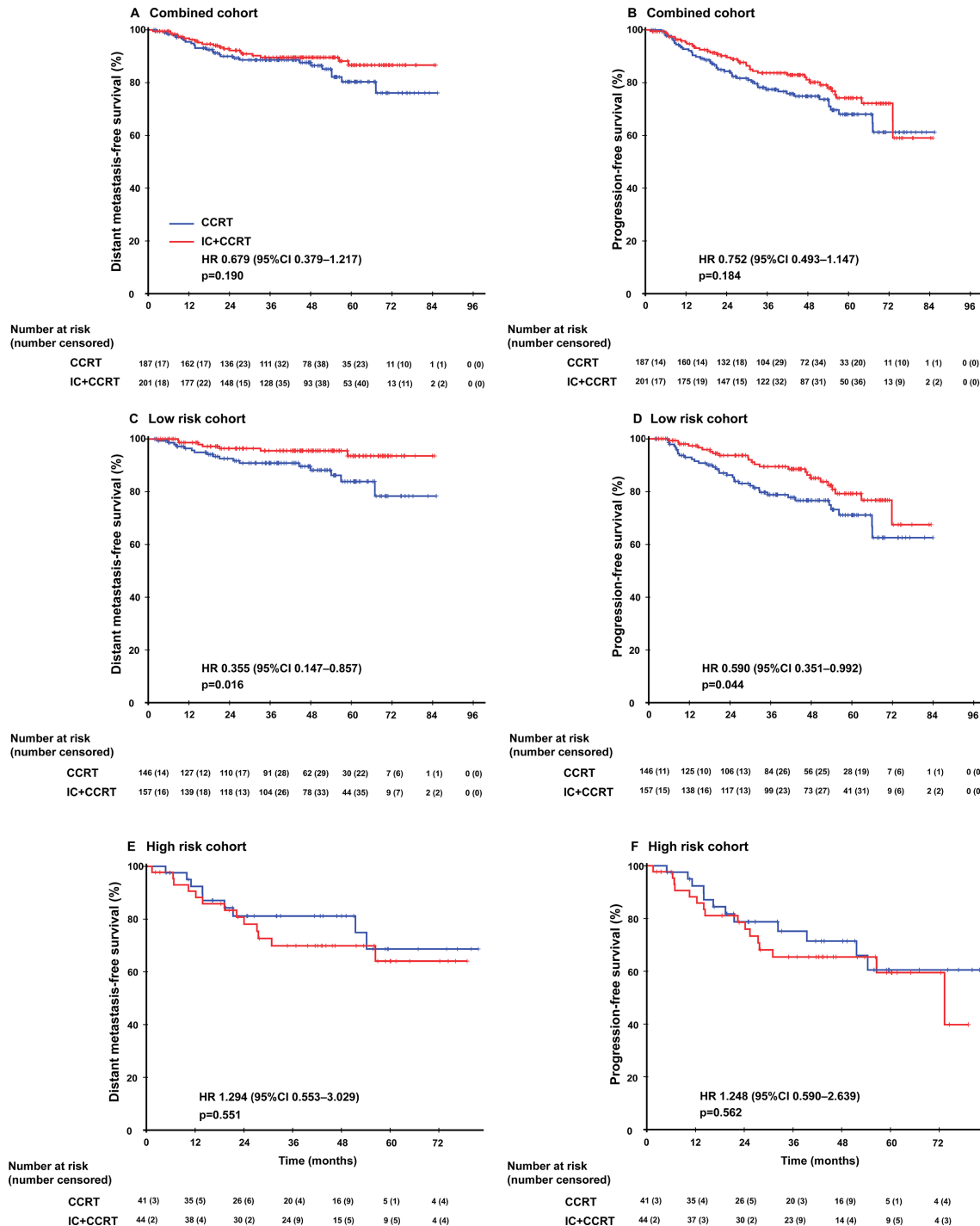
Figure 3 Kaplan-Meier survival curves between IC+CCRT and CCRT alone in different groups. Distant metastasis-free survival (A) and progression-free survival (B) for the whole combined cohort; distant metastasis-free survival (C) and progression-free survival (D) for the immune signature-defined low-risk patients in the combined cohort; distant metastasis-free survival (E) and progression-free survival (F) for the immune signature-defined high-risk patients in the combined cohort. We calculated p values using the unadjusted log-rank test and HRs using a univariate Cox regression analysis. CCRT, concurrent chemoradiotherapy; IC, induction chemotherapy.

Lin et al[33] demonstrated that the prognosis of patients with NPC could be distinguished by EBV DNA levels with a cut-off point of 1500 copies/mL. Previous studies showed that plasma EBV DNA level was considered the most potential biomarker to complement the TNM stage,[34] and we developed a nomogram B on the basis of

training cohort using plasma EBV DNA status, N stage, HGB, and immune signature A (online supplementary figure 4). Both nomogram A and nomogram B boosted higher predictive value compared with that of EBV DNA level or N category in the training cohort (online supplementary table S8). Nonetheless, the addition of EBV DNA

Table 2 Multivariable Cox regression analysis of prognostic factors in the training cohort and validation cohort

	HR* (95% CI)	P value
Distant metastasis-free survival		
Training cohort (n=194)		
HGB (≥130 vs <130 g/L)	0.335 (0.126 to 0.890)	0.028
N category (2–3 vs 0–1)	2.522 (1.086 to 5.857)	0.031
Immune signature (high vs low)	6.295 (2.886 to 13.729)	<0.001
Validation cohort (n=304)		
Age (≥45 years vs <45 years)	3.003 (1.355 to 6.654)	0.007
N stage (N2–3 vs N0–1)	3.461 (1.501 to 7.979)	0.004
Immune signature (high vs low)	4.297 (2.182 to 8.461)	<0.001
Progression-free survival		
Training cohort (n=194)		
N category (2–3 vs 0–1)	2.136 (1.107 to 4.118)	0.024
Immune signature (high vs low)	2.775 (1.484 to 5.189)	0.001
Validation cohort (n=304)		
HGB (≥130 vs <130 g/L)	0.535 (0.325 to 0.878)	0.013
Age (≥45 years vs <45 years)	2.018 (1.194 to 3.411)	0.009
N stage (N2–3 vs N0–1)	1.713 (1.028 to 2.854)	0.045
Immune signature (high vs low)	2.115 (1.289 to 3.469)	0.003

HRs and p values were calculated using an adjusted multivariate Cox proportional hazards regression model, immune signature (high risk vs low risk), gender (male vs female), age (≥45 years vs <45 years), T stage (T3–4 vs T1–2), N stage (N2–3 vs N0–1), overall stage (I–III vs IV), ECOG (0 vs 1 vs 2), LDH (≥245 vs <245 U/L), CRP (≥3 vs <3 mg/L), HGB (≥130 vs <130 g/L), and BMI (≥23 vs <23 kg/m²) were included as covariates. Variables were selected with the backward stepwise approach, and the p value threshold was 0.1 (p>0.1) for removing insignificant variables from the model. Only variables significantly associated with survival were presented, and marginally significant variables (0.05<p<0.1) were remained in the final Cox model but not presented in the table.
BMI, body mass index; CRP, serum C reactive protein; ECOG, Eastern Cooperative Oncology Group; HGB, hemoglobin; LDH, serum lactate dehydrogenase.

to nomogram B (C-index 0.805, 95% CI 0.718 to 0.892) did not enhance the accuracy compared with nomogram A (C-index 0.791, 95% CI 0.720 to 0.862; p=0.386) (online supplementary table S8). The EBV DNA data was unavailable in the validation cohort, thus it was used only to compare the sensitivity and specificity of the nomogram A with N category (online supplementary table S8).

DISCUSSION

By using fluorescent multiplex IHC and automated quantitation technology, which showed strong repeatability and reproducibility between different batches, this study developed and validated an objective immune signature tool, with four intratumor markers incorporated, the infiltration of CD163+ macrophage cells expressing PD-L1, and the expression of CD117 and CXCR5. The

combination of them categorized patients into high risk and low risk with significantly different DMFS. In addition, patients identified as low risk by the immune signature could benefit more from IC+CCRT.

The prognostic value of PD-L1 in NPC remains controversial. Zhu *et al* reported that PD-L1 expression on tumor cells was associated with favorable prognosis in a subgroup of patients with NPC who exhibited pre-existing lymphocytes infiltrating in tumor.[18] A study conducted by Fang demonstrated that PD-L1 was associated with worse disease-free survival in patients with NPC,[35] while Chan reported the insufficient prognostic value of PD-L1 expression.[36] The predictive effect of PD-L1 may be partly determined by the different expression of it in immune cells or tumor cells.[37] In this study, we demonstrated that more expression of PD-L1 on intratumor CD163+macrophages was associated with distant metastasis, which was consistent with previous study.[38] In recent years, PD-1 and PD-L1 therapies have shown remarkable clinical efficacy in numerous advanced solid cancers.[39–41] However, response rate of anti-PD-1/PD-L1 treatment in patients with recurrent or metastatic NPC only ranged from 20% to 34%.[42–44] It was crucial to identify effective indicators for predicting efficacy of PD-1 and PD-L1 therapies. Previous studies reported about the potential indispensable role of PD-L1 expressed by non-tumor cells on PD-L1 blockade-mediated tumor elimination in murine tumor models and the correlation between PD-L1-positive macrophages and the positive effects of anti-PD-L1 and anti-PD-1 antibodies in lung cancers and melanoma.[45–47] Our study might offer a clue to select intratumor PD-L1-positive macrophages as promising biomarker for the use of checkpoint inhibitors.

MCs migrated to the tumor microenvironment in response to stem cell factors secreted by tumor cells. Data suggested that CD117+ MCs promoted tumor progression by suppressing the immune system and also in several other ways.[48] It has also been reported that increased MC number correlated with an adverse prognosis.[49] Similar association between high CXCR5 expression and poorer prognosis was also observed in previous study in a variety of cancers.[50 51] Consistent with previous studies, our results showed that high expression of CD117, CXCR5 were associated with poorer prognosis in patients with NPC, which were worth to be considered as future antitumor targets.

Furthermore, our results showed that patients classified as low risk instead of high risk would benefit from IC+CCRT, that is, induction chemotherapy might not be effective enough for high-risk group to eradicate micrometastasis, and more aggressive therapeutic strategies should be considered in this cohort. Patients classified as high risk by the immune signature were believed to have abundant infiltrating immune cells along with elevated level of checkpoint markers, and that indicated that immunotherapy might work well in this population. In brief, the developed immune signature can be applied not only as a prognostic tool but also as a guidance for giving individualized antitumor treatment, such
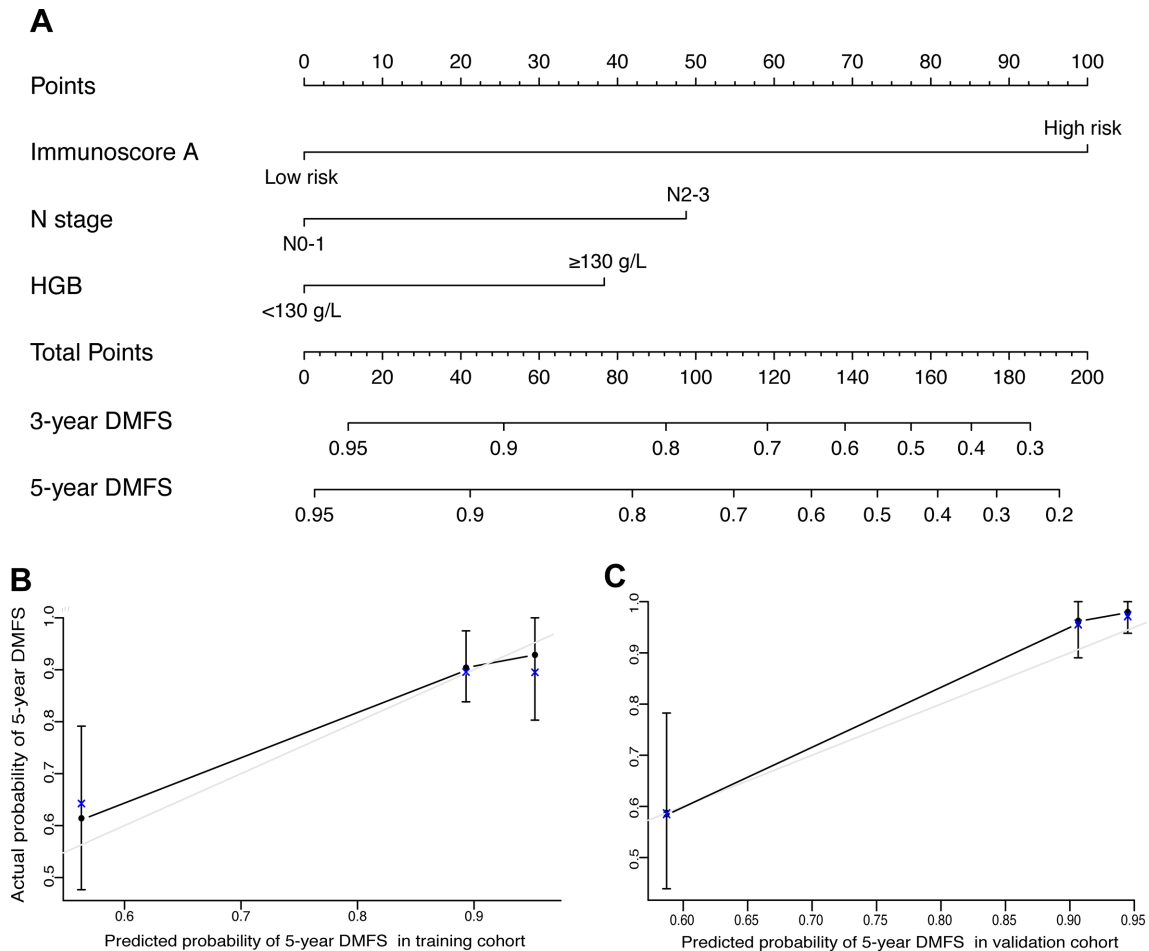
Figure 4 Nomogram A to predict the risk of distant metastasis in nasopharyngeal carcinoma (A). Calibration curves of the nomogram to predict DMFS at 5 years in: (B) the training cohort and (C) the external validation cohort. The actual DMFS was plotted on the y-axis and the nomogram predicted probability was plotted on the x-axis. HGB, hemoglobin; DMFS, distant metastasis-free survival.

as choosing appropriate candidates for induction chemotherapy. However, as the above views are yet theoretical conjecture, it is necessary to carry out prospective clinical trials to verify the applicability of our research results in clinical practice.

To provide a more accurate profile to predict the accurate risk of distant metastasis for each patient, nomograms were built. Nomogram A, with N stage, HGB, and immune signature A incorporated had an excellent predictive accuracy, and nomogram B was formed on the basis of nomogram A with the addition of EBV DNA level. However, the complement of EBV DNA to nomogram A did not enhance the accuracy of nomogram B, which may be explained by the existence of potential correlation between EBV and immune features, as it was reported that 69% EBV-related NPC exhibited high expression of PD-L1.[52] On the other hand, since EBV DNA detection methods varied among institutes, the generalization of nomogram B including EBV DNA might be hindered. Thus, nomogram A, which showed same accuracy, was worth to be popularized for predicting prognosis for locally advanced NPC. In addition, we have also tried the LASSO Cox regression model to build the immune

signature and found that only one marker in intratumor was selected (CD117), which had similar prognostic value with immune signature A built by LASSO logistic regression (ROC 0.711, 95% CI 0.580 to 0.843 vs ROC 0.668, 95% CI 0.478 to 0.858; p=0.618) concerning time-independent 5-year ROC. In spite of the handy nature of one single marker in clinic, the combined immune signature built by LASSO logistic regression model (percentage of PD-L1+ CD163+, CXCR5, CD117) could reveal more information about immune status and offer insight into the immunotherapy of patients with NPC.

The present study had several limitations. First, the data were obtained in NPC-endemic area in China, and the pathological subtype was mainly undifferentiated non-keratinizing carcinoma. The application of it in areas with distinct pathological subtypes and clinical characteristics should be revalidated. Second, the number of immune markers screened in the training cohort was limited, which resulted in a smaller panel of genes being integrated into the immune signature compared with other gene expression profiling studies such as complementary DNA arrays. Third, the number of fluorescent channels of the multiplexed immunofluorescence staining was limited by the

overlap of fluorescent signals, thus all markers into one panel and their multiple combinations are difficult to put into practice. Fourth, the NPC tissue was obtained by biopsy forceps and it was hard to get the whole tumor. We evaluated the expression of each immune marker on single biopsy, which might not be representative enough to reflect the integrated immune pattern of patients with NPC because of the possible tumor heterogeneity. Fifth, confined to the sample size and follow-up duration, many patients who had tumor progression were still alive with tumor burden, thus the prediction efficiency for overall survival (OS) was not as good as those for distant metastasis and progression. Further studies with more patients and longer follow-up times would be useful to evaluate the impact of immune signature on OS. Furthermore, we did not explore the value of the immune signature as a predictive tool to identify patients who would benefit from immunotherapy in clinical practice. Therefore, further studies were encouraged to explore the value of the immune signature for identifying candidates for immunotherapy, and the validation by prospective studies from other NPC-endemic areas were also expected.

CONCLUSION

Our findings showed that the prognostic tool comprising a multiplexed quantitative fluorescence-based objective immune signature could effectively classify locoregionally advanced patients with NPC into different risk groups for distant metastasis. Moreover, we showed that patients identified as low risk using the developed immune signature tool could benefit more from IC+CCRT. The immune signature-derived nomogram could provide clinicians with practical and accessible information for predicting prognosis.

Author affiliations
[1]Sun Yat-sen University Cancer Center, State Key Laboratory of Oncology in South China, Collaborative Innovation Center for Cancer Medicine, Guangdong Key Laboratory of Nasopharyngeal Carcinoma Diagnosis and Therapy, Guangzhou, Guangdong Province, People's Republic of China
[2]Department of Nasopharyngeal Carcinoma, Sun Yat-sen University Cancer Center, Guangzhou, Guangdong Province, People's Republic of China
[3]Department of Pathology, Sun Yat-Sen Memorial Hospital, Guangzhou, Guangdong Province, People's Republic of China
[4]Department of Pathology, Sun Yat-sen University Cancer Center, Guangzhou, Guangdong Province, People's Republic of China

ORCID iD
Hai-Qiang Mai http://orcid.org/0000-0003-0214-203X

REFERENCES

1 Torre LA, Bray F, Siegel RL, *et al*. Global cancer statistics, 2012. *CA Cancer J Clin* 2015;65:87–108.
2 Wee JTS, Ha TC, Loong SLE, *et al*. Is nasopharyngeal cancer really a "Cantonese cancer"? *Chin J Cancer* 2010;29:517–26.
3 Pan JJ, Ng WT, Zong JF, *et al*. Prognostic nomogram for refining the prognostication of the proposed 8th edition of the AJCC/UICC staging system for nasopharyngeal cancer in the era of intensity-modulated radiotherapy. *Cancer* 2016;122:3307–15.
4 Lai S-Z, Li W-F, Chen L, *et al*. How does intensity-modulated radiotherapy versus conventional two-dimensional radiotherapy influence the treatment results in nasopharyngeal carcinoma patients? *Int J Radiat Oncol Biol Phys* 2011;80:661–8.
5 Pagès F, Mlecnik B, Marliot F, *et al*. International validation of the consensus immunoscore for the classification of colon cancer: a prognostic and accuracy study. *Lancet* 2018;391:2128–39.
6 Fridman WH, Pagès F, Sautès-Fridman C, *et al*. The immune contexture in human tumours: impact on clinical outcome. *Nat Rev Cancer* 2012;12:298–306.
7 Galon J, Angell HK, Bedognetti D, *et al*. The continuum of cancer immunosurveillance: prognostic, predictive, and mechanistic signatures. *Immunity* 2013;39:11–26.
8 Jain A, Chia WK, Toh HC. Immunotherapy for nasopharyngeal cancer-a review. *Chin Clin Oncol* 2016;5:22.
9 Yu Y, Ke L, Lv X, *et al*. The prognostic significance of carcinoma-associated fibroblasts and tumor-associated macrophages in nasopharyngeal carcinoma. *Cancer Manag Res* 2018;10:1935–46.
10 Chen X, Li X, Zhao F, *et al*. [Distribution and prognostic significance of tumor-infiltrating mast cells in nasopharyngeal carcinoma]. *Zhonghua Er Bi Yan Hou Tou Jing Wai Ke Za Zhi* 2015;50:306–11.
11 Li Y-W, Qiu S-J, Fan J, *et al*. Intratumoral neutrophils: a poor prognostic factor for hepatocellular carcinoma following resection. *J Hepatol* 2011;54:497–505.
12 Luen SJ, Salgado R, Fox S, *et al*. Tumour-Infiltrating lymphocytes in advanced HER2-positive breast cancer treated with pertuzumab or placebo in addition to trastuzumab and docetaxel: a retrospective analysis of the CLEOPATRA study. *Lancet Oncol* 2017;18:52–62.
13 Wang Y-Q, Chen Y-P, Zhang Y, *et al*. Prognostic significance of tumor-infiltrating lymphocytes in nondisseminated nasopharyngeal carcinoma: a large-scale cohort study. *Int J Cancer* 2018;142:2558–66.
14 Freeman GJ, Long AJ, Iwai Y, *et al*. Engagement of the PD-1 immunoinhibitory receptor by a novel B7 family member leads to negative regulation of lymphocyte activation. *J Exp Med* 2000;192:1027–34.

15 Boenisch O, D'Addio F, Watanabe T, *et al*. TIM-3: a novel regulatory molecule of alloimmune activation. *J Immunol* 2010;185:5806–19.

16 Wang J, Sanmamed MF, Datar I, *et al*. Fibrinogen-Like protein 1 is a major immune inhibitory ligand of LAG-3. *Cell* 2019;176:e12:334–47.

17 Gandhi MK, Moll G, Smith C, *et al*. Galectin-1 mediated suppression of Epstein-Barr virus specific T-cell immunity in classic Hodgkin lymphoma. *Blood* 2007;110:1326–9.

18 Zhu Q, Cai M-Y, Chen C-L, *et al*. Tumor cells PD-L1 expression as a favorable prognosis factor in nasopharyngeal carcinoma patients with pre-existing intratumor-infiltrating lymphocytes. *Oncoimmunology* 2017;6:e1312240.

19 Ono T, Azuma K, Kawahara A, *et al*. Prognostic stratification of patients with nasopharyngeal carcinoma based on tumor immune microenvironment. *Head Neck* 2018;40:2007–19.

20 Turley SJ, Cremasco V, Astarita JL. Immunological hallmarks of stromal cells in the tumour microenvironment. *Nat Rev Immunol* 2015;15:669–82.

21 Tumeh PC, Harview CL, Yearley JH, *et al*. Pd-1 blockade induces responses by inhibiting adaptive immune resistance. *Nature* 2014;515:568–71.

22 Carey CD, Gusenleitner D, Lipschitz M, *et al*. Topological analysis reveals a PD-L1-associated microenvironmental niche for Reed-Sternberg cells in Hodgkin lymphoma. *Blood* 2017;130:2420–30.

23 Jiang F, Yu W, Zeng F, *et al*. Pd-1 high expression predicts lower local disease control in stage IV M0 nasopharyngeal carcinoma. *BMC Cancer* 2019;19:503.

24 Anderson AC. TIM-3: an emerging target in the cancer immunotherapy landscape. *Cancer Immunol Res* 2014;2:393–8.

25 Nguyen LT, Ohashi PS. Clinical blockade of PD1 and LAG3--potential mechanisms of action. *Nat Rev Immunol* 2015;15:45–56.

26 Miksch RC, Schoenberg MB, Weniger M, *et al*. Prognostic impact of tumor-infiltrating lymphocytes and neutrophils on survival of patients with upfront resection of pancreatic cancer. *Cancers* 2019;11:39.

27 Tanis E, Julié C, Emile J-F, *et al*. Prognostic impact of immune response in resectable colorectal liver metastases treated by surgery alone or surgery with perioperative FOLFOX in the randomised EORTC study 40983. *Eur J Cancer* 2015;51:2708–17.

28 Zhang J, Fang W, Qin T, *et al*. Co-Expression of PD-1 and PD-L1 predicts poor outcome in nasopharyngeal carcinoma. *Med Oncol* 2015;32:86.

29 Ooft ML, van Ipenburg JA, Sanders ME, *et al*. Prognostic role of tumour-associated macrophages and regulatory T cells in EBV-positive and EBV-negative nasopharyngeal carcinoma. *J Clin Pathol* 2018;71:267–74.

30 Chen T-C, Chen C-H, Wang C-P, *et al*. The immunologic advantage of recurrent nasopharyngeal carcinoma from the viewpoint of Galectin-9/Tim-3-related changes in the tumour microenvironment. *Sci Rep* 2017;7:10349.

31 Budwit-Novotny DA, McCarty KS, Cox EB, *et al*. Immunohistochemical analyses of estrogen receptor in endometrial adenocarcinoma using a monoclonal antibody. *Cancer Res* 1986;46:5419–25.

32 Camp RL, Dolled-Filhart M, Rimm DL. X-tile: a new bio-informatics tool for biomarker assessment and outcome-based cut-point optimization. *Clin Cancer Res* 2004;10:7252–9.

33 Lin J-C, Wang W-Y, Chen KY, *et al*. Quantification of plasma Epstein-Barr virus DNA in patients with advanced nasopharyngeal carcinoma. *N Engl J Med* 2004;350:2461–70.

34 Leung S-fai, Zee B, Ma BB, *et al*. Plasma Epstein-Barr viral deoxyribonucleic acid quantitation complements tumor-node-metastasis staging prognostication in nasopharyngeal carcinoma. *J Clin Oncol* 2006;24:5414–8.

35 Fang W, Zhang J, Hong S, *et al*. EBV-driven LMP1 and IFN-γ up-regulate PD-L1 in nasopharyngeal carcinoma: implications for oncotargeted therapy. *Oncotarget* 2014;5:12189–202.

36 Chan OSH, Kowanetz M, Ng WT, *et al*. Characterization of PD-L1 expression and immune cell infiltration in nasopharyngeal cancer. *Oral Oncol* 2017;67:52–60.

37 Kluger HM, Zito CR, Turcu G, *et al*. Pd-L1 studies across tumor types, its differential expression and predictive value in patients treated with immune checkpoint inhibitors. *Clin Cancer Res* 2017;23:4270–9.

38 Xu-Monette ZY, Xiao M, Au Q, *et al*. Immune profiling and quantitative analysis decipher the clinical role of Immune-Checkpoint expression in the tumor immune microenvironment of DLBCL. *Cancer Immunol Res* 2019;7:644–57.

39 Hodi FS, O'Day SJ, McDermott DF, *et al*. Improved survival with ipilimumab in patients with metastatic melanoma. *N Engl J Med* 2010;363:711–23.

40 Powles T, Eder JP, Fine GD, *et al*. MPDL3280A (anti-PD-L1) treatment leads to clinical activity in metastatic bladder cancer. *Nature* 2014;515:558–62.

41 Hamid O, Robert C, Daud A, *et al*. Safety and tumor responses with lambrolizumab (anti-PD-1) in melanoma. *N Engl J Med* 2013;369:134–44.

42 Ma BBY, Lim W-T, Goh B-C, Hui EP, *et al*. Antitumor activity of nivolumab in recurrent and metastatic nasopharyngeal carcinoma: an international, multicenter study of the Mayo clinic phase 2 Consortium (NCI-9742). *J Clin Oncol* 2018;36:1412–8.

43 Hsu C, Lee S-H, Ejadi S, *et al*. Safety and antitumor activity of pembrolizumab in patients with programmed death-ligand 1-positive nasopharyngeal carcinoma: results of the KEYNOTE-028 study. *J Clin Oncol* 2017;35:4050–6.

44 Fang W, Yang Y, Ma Y, *et al*. Camrelizumab (SHR-1210) alone or in combination with gemcitabine plus cisplatin for nasopharyngeal carcinoma: results from two single-arm, phase 1 trials. *Lancet Oncol* 2018;19:1338–50.

45 Herbst RS, Soria J-C, Kowanetz M, *et al*. Predictive correlates of response to the anti-PD-L1 antibody MPDL3280A in cancer patients. *Nature* 2014;515:563–7.

46 Vilain RE, Menzies AM, Wilmott JS, *et al*. Dynamic changes in PD-L1 expression and immune infiltrates early during treatment predict response to PD-1 blockade in melanoma. *Clin Cancer Res* 2017;23:5024–33.

47 Watanabe H, Ohashi K, Nishii K, *et al*. A long-term response to nivolumab in a case of PD-L1-negative lung adenocarcinoma with an <i>EGFR</i> mutation and surrounding PD-L1-positive tumor-associated macrophages. *Intern Med* 2019;58:3033–7.

48 Ribatti D. Mast cells as therapeutic target in cancer. *Eur J Pharmacol* 2016;778:152–7.

49 Fu H, Zhu Y, Wang Y, *et al*. Identification and validation of stromal immunotype predict survival and benefit from adjuvant chemotherapy in patients with muscle-invasive bladder cancer. *Clin Cancer Res* 2018;24:3069–78.

50 Zheng Z, Cai Y, Chen H, *et al*. CXCL13/CXCR5 axis predicts poor prognosis and promotes progression through PI3K/Akt/mTOR pathway in clear cell renal cell carcinoma. *Front Oncol* 2018;8:682.

51 Zhu Z, Zhang X, Guo H, *et al*. CXCL13-CXCR5 axis promotes the growth and invasion of colon cancer cells via PI3K/Akt pathway. *Mol Cell Biochem* 2015;400:287–95.

52 Larbcharoensub N, Mahaprom K, Jiarpinitnun C, *et al*. Characterization of PD-L1 and PD-1 expression and CD8+ tumor-infiltrating lymphocyte in Epstein-Barr virus-associated nasopharyngeal carcinoma. *Am J Clin Oncol* 2018;41:1204–10.